ADVANCED FUNCTIONAL MATERIALS
www.afm-journal.de

www.MaterialsViews.com

Optimizing the Size of Micellar Nanoparticles for Efficient siRNA Delivery

Shi Liang, Xian-Zhu Yang, Xiao-Jiao Du, Hong-Xia Wang, Hong-Jun Li, Wei-Wei Liu, Yan-Dan Yao, Yan-Hua Zhu, Yin-Chu Ma, Jun Wang,* and Er-Wei Song**

Delivery of small interfering RNA (siRNA) by nanocarriers has shown promising therapeutic potential in cancer therapy. However, poor understanding of the correlation between the physicochemical properties of nanocarriers and their interactions with biological systems has significantly hindered its anticancer efficacy. Herein, in order to identify the optimal size of nanocarriers for siRNA delivery, different sized cationic micellar nanoparticles (MNPs) (40, 90, 130, and 180 nm) are developed that exhibit similar siRNA binding efficacies, shapes, surface charges, and surface chemistries (PEGylation) to ensure size is the only variable. Size-dependent biological effects are carefully and comprehensively evaluated through both in vitro and in vivo experiments. Among these nanocarriers, the 90 nm MNPs show the optimal balance of prolonged circulation and cellular uptake by tumor cells, which result in the highest retention in tumor cells. In contrast, larger MNPs are rapidly cleared from the circulation and smaller MNPs are inefficiently taken up by tumor cells. Accordingly, 90 nm MNPs carrying polo-like kinase 1 (Plk1)-specific siRNA (siPlk1) show superior antitumor efficacy, indicating that 90 nm could either be the optimal size for systemic delivery of siRNA or close to it. Our findings provide valuable information for rationally designing nanocarriers for siRNA-based cancer therapy in the future.

1. Introduction

Since the discovery of RNA interference by Fire et al.,[1] small interfering RNA (siRNA) has emerged as a powerful therapeutic agent for cancer therapy because of its ability to silence specific genes rapidly and efficiently.[2–4] Up to now, a number of nanocarriers capable of systemic delivery of siRNA to tumor tissues and cells in vivo have been described.[5,6] Among these delivery systems, positively charged nanoparticles were the most common formulations, which could efficiently carry siRNA through electrostatic interactions and show promising efficacy in cancer therapy.[7–14] These nano-delivery systems can accumulate in solid tumors through the enhanced permeability and retention (EPR) effect, subsequently be taken up by the tumor cells, and then further suppress tumor growth by specifically silencing the expression of oncogenes.[15,16] Numerous researchers have been heavily focused on the synthesis of novel nanomaterials for siRNA-based therapeutics.[17–21] However, poor understanding of the correlation between the physicochemical properties of nanocarriers and their interactions with biological systems has significantly hindered their anticancer efficacy. To achieve superior anticancer activities, it is essential to investigate this correlation in order to establish principles for the rational design of nanocarriers for siRNA-based therapeutics. Unfortunately, relevant researches have been rarely reported.

To date, many groups have demonstrated how the physicochemical properties of nanodelivery systems of small molecular chemotherapeutic drugs interact with biological systems, including their size, shape, surface charge, and surface coating.[22–26] As a part of this effort, previous studies have shown that the size of the delivery system had a critical effect on its in vivo fate, including clearance, biodistribution, cellular uptake, penetration, and overall therapeutic efficacy against cancers.[27–30] Kataoka and Cheng's groups separately

Dr. S. Liang, Prof. Y.-D. Yao, Prof. E.-W. Song
Breast Tumor Center
Sun Yat-sen Memorial Hospital
Sun Yat-sen University
Guangzhou 510120, P. R. China
E-mail: songew@mail.sysu.edu.cn
Prof. X.-Z. Yang, Dr. X.-J. Du, Dr. H.-X. Wang, H.-J. Li, W.-W. Liu, Y.-H. Zhu, Prof. J. Wang
Hefei National Laboratory for Physical Sciences at Microscale and School of Life Sciences
University of Science and Technology of China
Hefei, Anhui 230027, P. R. China
E-mail: yangxz@hfut.edu.cn; jwang699@ustc.edu.cn
Prof. X.-Z. Yang, Y.-C. Ma
Department of Medical Materials and Rehabilitation Engineering
School of Medical Engineering
Hefei University of Technology
Hefei, Anhui 230009, P. R. China
Prof. J. Wang
The CAS Key Laboratory of Innate Immunity and Chronic Disease
School of Life Sciences and Medical Center
University of Science and Technology of China
Hefei, Anhui 230027, P. R. China

DOI: 10.1002/adfm.201501548

© 2015 WILEY-VCH Verlag GmbH & Co. KGaA, Weinheim

demonstrated that 50 nm nanoparticles could be the optimal size nano-delivery system for small molecular chemotherapeutic drugs.[31,32] To demonstrate this, both groups used neutral nanodelivery systems to avoid interference by surface charge, which could mean the determined optimal size for chemotherapeutic drugs was not appropriate for positively charged delivery systems for siRNA. Therefore, it is still essential to determine the optimal size of siRNA-based nanocarriers for cancer therapy.

In this study, we used multiple preparations of cationic mixed micellar nanoparticles (MNPs) that possessed identical physiochemical properties, except for size in order to investigate optimal size for cancer therapy. On the basis of current knowledge and other reports, the optimum nanoparticle size for cancer therapy is between about 20 and 200 nm. Thus, to investigate the optimal size of nanocarriers for siRNA delivery, MNP sizes of 40, 90, 130, and 180 nm were developed by the rational design. After loaded siRNA, these differently sized MNP/siRNAs exhibited similar key physicochemical properties, including shape, zeta potentials, stability, and siRNA release rate, leaving size as the only variable to be studied for size effect. We systematically and comprehensively evaluated the size effect of these MNP/siRNAs on circulation, internalization, retention, and overall antitumor efficacy. Our results clearly demonstrated that the size of nanocarriers used for siRNA delivery plays a critical role in determining their biological properties and antitumor activity.

2. Results and Discussion

2.1. Preparation and Characterization of Different Sized Cationic MNPs

We have previously demonstrated that cationic mixed micellar nanoparticles (MNPs) self-assembled from two diblock copolymers of poly(ε-caprolactone)-*b*-poly(2-aminoethyl ethylene phosphate) (PCL-*b*-PPEEA) and poly(ethylene glycol)-*b*-poly(ε-caprolactone) (mPEG-*b*-PCL) were capable of binding siRNA to form a micelle/siRNA complex.[33] Herein, in order to prepare different sized MNPs for siRNA delivery, we prepared the nanoparticles by a dialysis method using a mixture of mPEG-*b*-PCL, PCL-*b*-PPEEA, and the PCL homopolymer; the molar ratio of mPEG-*b*-PCL and PCL-*b*-PPEEA was fixed at 1.5:1.0, and that of the PCL homopolymer was gradually increased (Figure S1, Supporting Information). As shown in Figure S2 (Supporting Information), the particle volume of the MNPs, which was calculated according to the formula: particle volume (mm^3) = $1/6 \times \pi \times$ diameter^3, increased linearly with the molar ratio of [PCL] from the PCL homopolymer/[PCL], mPEG-*b*-PCL, and PCL-*b*-PPEEA. Thus, different sized MNPs could be prepared by this method and MNPs with diameters of 40, 90, 130, to 180 nm were obtained for the subsequent experiments (**Figure 1**A). These MNPs were denoted as MNP-40, MNP-90, MNP-130, and MNP-180, respectively. In addition, the polydispersity index (PDI) of these MNPs was 0.193, 0.085, 0.124, and 0.111, respectively, indicating narrow size distribution of the obtained MNPs. The transmission electron microscope (TEM) images of these MNP (Figure S3, Supporting Information) show the micelles took on a classic spherical micelle structure, indicating the similar shapes of the different MNP preparations.

To demonstrate the critical micellization concentrations (CMC) of the different sized MNPs, the excitation spectra of pyrene were measured with increased concentration of MNPs according to a previously reported method.[34] As shown in Figure S4 (Supporting Information), these MNPs presented

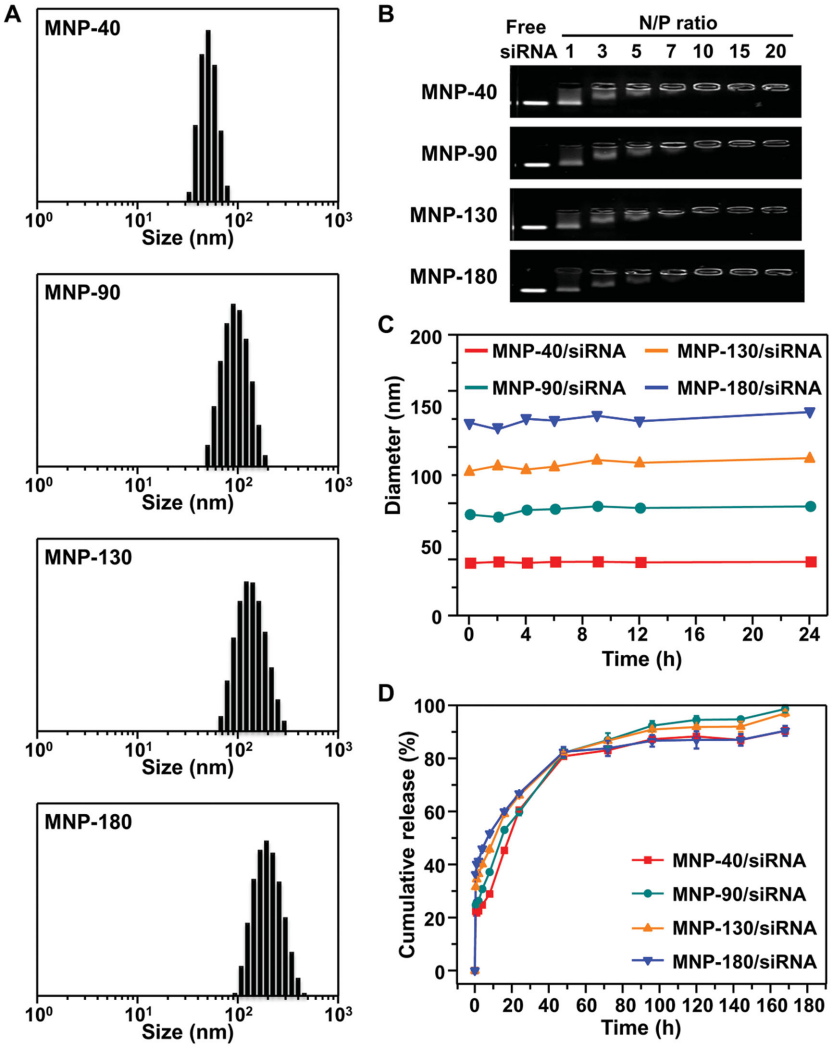

Figure 1. A) Dynamic light scattering measurements of cationic mixed micellar nanoparticles. B) Binding affinity of different sized MNPs to siRNA at different N:P ratios demonstrated by gel retardation assay. C) Changes in size of the MNP/siRNAs following incubation with DMEM containing 10% FBS. D) Cumulative amount of siRNA released from different sized MNPs.

© 2015 WILEY-VCH Verlag GmbH & Co. KGaA, Weinheim

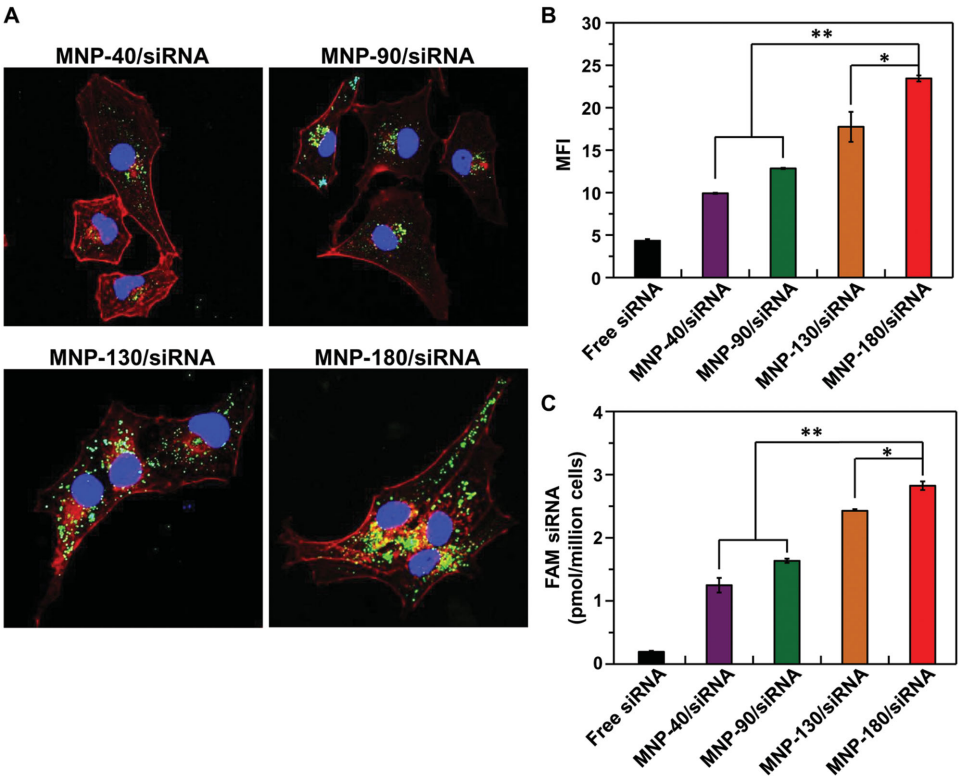

Figure 2. A) Confocal laser scanning microscope (CLSM) images of cellular uptake of different sized MNP/FAM-siRNAs (N:P = 10:1) (green) in MDA-MB-231 cells after 6 h of incubation. Cytoskeletal F-actin (red) and cell nuclei (blue) were counterstained with Alexa Fluor 568 phalloidin and DAPI, respectively. B) Flow cytometric analyses of MDA-MB-231 cells after 6 h of incubation with different sized MNP/FAM-siRNA complexes. C) Total siRNA accumulation in MDA-MB-231 cells after incubation with different sized MNP/FAM-siRNAs for 6 h. The final concentration of FAM-siRNA in the culture medium was 200×10^{-9} M in the experiments. $^{*}p < 0.05$, $^{**}p < 0.01$ ($n = 3$).

similar CMCs (all around 8.0 mg L^{-1}). In addition, even at the higher concentrations, these MNPs did not exhibit significant cytotoxicity to the cancer cells (Figure S5, Supporting Information), indicating the toxicity of the MNPs would not interfere with the in vitro and in vivo results.

The cationic MNP-40, MNP-90, MNP-130, and MNP-180 all showed similar zeta potentials, ranging from 32.3 to 40.2 mV, which allows for the binding of siRNA. As demonstrated by a gel retardation assay, efficient siRNA binding to these cationic MNPs (Figure 1B) occurred at a molar ratio of the PPEEA nitrogen to the siRNA phosphate (N:P) of 5:1. To obtain similar zeta potentials in the siRNA-loaded MNPs, the siRNA was loaded at an N:P ratio of 10:1 for the subsequent experiment. Note that the average size of each MNP was almost unchanged (Figure S6, Supporting Information) after siRNA loading. And, after incubation in DMEM medium with 10% fetal bovine serum (FBS) at 37 °C, different sized MNP/siRNAs maintained their diameters for over 24 h (Figure 1C), indicating the excellent colloidal stability of the different sized MNP/siRNAs. In addition, to demonstrate the size effect on siRNA release rate, fluorescent FAM-labeled siRNA was used and the FAM-siRNA concentration in the supernatant was analyzed according to the previously reported method.[35] As shown in Figure 1D, within the initial 12 h, the siRNA release rate increased as the diameter of the MNP/siRNAs increased. After 48 h incubation in phosphate buffer saline (PBS), the released siRNA from the MNP/siRNA all reached ≈80%, showing a similar total release. The above results demonstrated that these differently sized MNPs with siRNA loading exhibited similar physicochemical properties, including shape, zeta potentials, stability, and siRNA release rate.

2.2. Increasing the Size of MNP/siRNAs Enhances the Cellular Uptake of siRNA

To demonstrate the size effect of the siRNA-loaded MNPs on cellular uptake, MDA-MB-231 tumor cells were incubated with different sized MNP/siRNAs. Fluorescent FAM-labeled siRNA (green fluorescence) was used to highlight the nanoparticles. After 6 h of incubation, we counterstained cytoskeletal F-actin and the cell nuclei with Alexa Fluor 568 phalloidin and 6-diamidino-2-phenylindole (DAPI), respectively. As shown in **Figure 2**A, the cells incubated with MNP-180/siRNA exhibited much stronger intracellular green fluorescence signals in the cytoplasm compared to the cells treated with other sized MNP/siRNAs, and the result indicated that cellular uptake of the MNP/siRNAs increased with increasing size. This size-dependent cellular uptake was further corroborated by flow cytometry analyses. As shown in Figure 2B, after incubation for 6 h, the intensity of intracellular fluorescence after incubation with MNP-180 was significantly stronger than those of

© 2015 WILEY-VCH Verlag GmbH & Co. KGaA, Weinheim

MNP-40 and MNP-90 ($P < 0.01$), and slightly stronger than that of MNP-130 ($P < 0.05$) (Figure 2B). Moreover, to precisely determine the amount of intracellular siRNA following incubation with different sized MNP/siRNAs, we established a quantitative method to detect the intracellular siRNA. After 6 h of incubation, the cells were lysed with 1% Triton X-100 and the supernatants were collected for high-performance liquid chromatography (HPLC) analyses according to our previously reported method.[36] As shown in Figure 2C, the amount of intracellular FAM-siRNA following incubation with MNP-40, MNP-90, MNP-130, and MNP-180 was 1.25 ± 0.12 pmol/million cells, 1.64 ± 0.03 pmol/million cells, 2.43 ± 0.01 pmol/million cells, and 2.83±0.07 pmol/million cells, respectively. This phenomenon was consistent with the confocal laser scanning microscopy (CLSM) and flow cytometry results, indicating that uptake of the siRNA by MDA-MB-231 tumor cells increased with increasing size of the MNP/siRNAs.

2.3. Larger MNP/siRNAs Utilize an Additional Endocytosis Pathway

To understand the reason behind size-dependent cellular uptake, we next determined the entry mechanism of these MNP/siRNAs. It has been reported that endocytosis is the major means via which nanoparticles enter cells, which is an energy-dependent mechanism.[37–39] As shown in **Figure 3**, incubating different sized MNP/siRNAs with MDA-MB-231 cells at 4 °C significantly inhibited the cellular uptake of all nanoparticles, suggesting that endocytosis is the main cellular uptake pathway for these different sized MNP/siRNAs. Furthermore, to discriminate among distinct endocytosis pathway subcategories (including clathrin-mediated endocytosis, caveolae-mediated endocytosis, macro-pinocytosis), we used different inhibitors and then examined the intracellular FAM-siRNA fluorescence intensity. As shown in Figure 3, inhibition of clathrin-mediated endocytosis with sucrose significantly decreased intracellular FAM-siRNA fluorescence intensity for all the different sized MNP/siRNAs (reductions up to ≈70%). Pretreatment of the cells with filipin, a specific inhibitor of caveolae-dependent endocytosis, prior to incubation with MNP/siRNAs also had a significant impact on their uptake by MDA-MB-231 cells, resulting in 16.0%, 15.1%, 30.4%, and 41.8% reductions for MNP-40/siRNA, MNP-90/siRNA, MNP-130/siRNA, and MNP-180/siRNA, respectively. However, inhibiting macropinocytosis with wortmannin did not decrease the cellular uptake of MNP-40/siRNA and MNP-90/siRNA, while intracellular fluorescence following incubation with MNP-130/siRNA and MNP-180/siRNA was decreased by 61.2% and 64.2%, respectively. These results reveal that the smaller nanoparticles MNP-40/siRNA and MNP-90/siRNA were internalized by MDA-MB-231 cells via clathrin and caveolae-dependent endocytosis but not macropinocytosis. In contrast, the larger sized MNP-130/siRNA and MNP-180/siRNA were also able to enter into cells by the macropinocytosis pathway. Thus, all three endocytotic pathways are involved in the uptake of MNP-130/siRNA and MNP-180/siRNA, with micropinocytosis being the major one, a fact that may contribute to size-dependent cellular uptake.

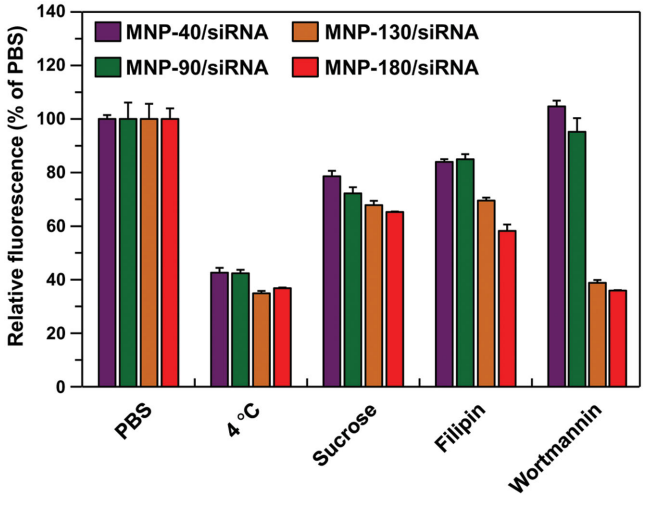

Figure 3. Flow cytometric analyses of the intracellular fluorescence intensity in MDA-MB-231 cells after 6 h of incubation with different sized MNP/siRNAs. Cells were incubated either at 37 °C (control) or at 4 °C. Prior to incubation with MNP/siRNAs at 37 °C, cells were pretreated with sucrose, filipin, or wortmannin.

2.4. Increased Size of MNP/siRNAs Enhances Gene Silencing Efficiency and Promotes Cell Apoptosis In Vitro

The enhanced cellular uptake of the larger MNP/siRNA may be accompanied by an improved silencing efficiency of target gene expression in the tumor cells. To demonstrate this, polo-like kinase 1 (Plk1), which is a well-known key regulator of mitotic progression in mammalian cells and is high-expressed in many cancer cells, was selected as the oncogenic target.[40,41] MDA-MB-231 cells were incubated with each different sized MNP carrying 200×10^{-9} M siPlk1 (MNP/siPlk1) for 24 h, and Plk1 gene expression was analyzed by quantitative real-time polymerase chain reaction (qRT-PCR). As shown in **Figure 4**A, the free siPlk1 did not downregulate Plk1 expression, while the positive control Lipofectamine RNAiMAX was able to significantly downregulate PLK1 expression, to 41.1%. Meanwhile, each of the different sized MNP/siPlk1 could efficiently downregulate Plk1 gene expression in MDA-MB-231 cells. As expected, the gene silencing efficiency of the MNP/siPlk1 was size-dependent; increasing the size of the MNP/siPlk1 enhanced the inhibition of gene expression. For example, MNP-40/siPlk1 and MNP-90/siPlk1 only showed 30.5 ± 3.4% and 37.0 ± 1.5% down-regulation of PLK1 mRNA expression, while MNP-130/siPlk1 and MNP-180/siPlk1 exhibited significantly improved gene silencing efficiency, achieving 42.2 ± 4.2% and 53.4 ± 1.9% down-regulation, respectively. In addition, it is noteworthy that none of the MNPs carrying siN.C. downregulated Plk1 protein expression (Figure S7A, Supporting Information), indicating that nonspecific gene silencing did not occur. Furthermore, western blot analyses were used to detect Plk1 protein levels after the cells were incubated for 48 h, and a similar size-dependent gene silencing phenomenon was detected in down-regulation of PLK1 protein expression (Figure 4B and Figure S7B, Supporting Information). The results demonstrated that increasing the size of the MNP/siRNA could significantly

© 2015 WILEY-VCH Verlag GmbH & Co. KGaA, Weinheim

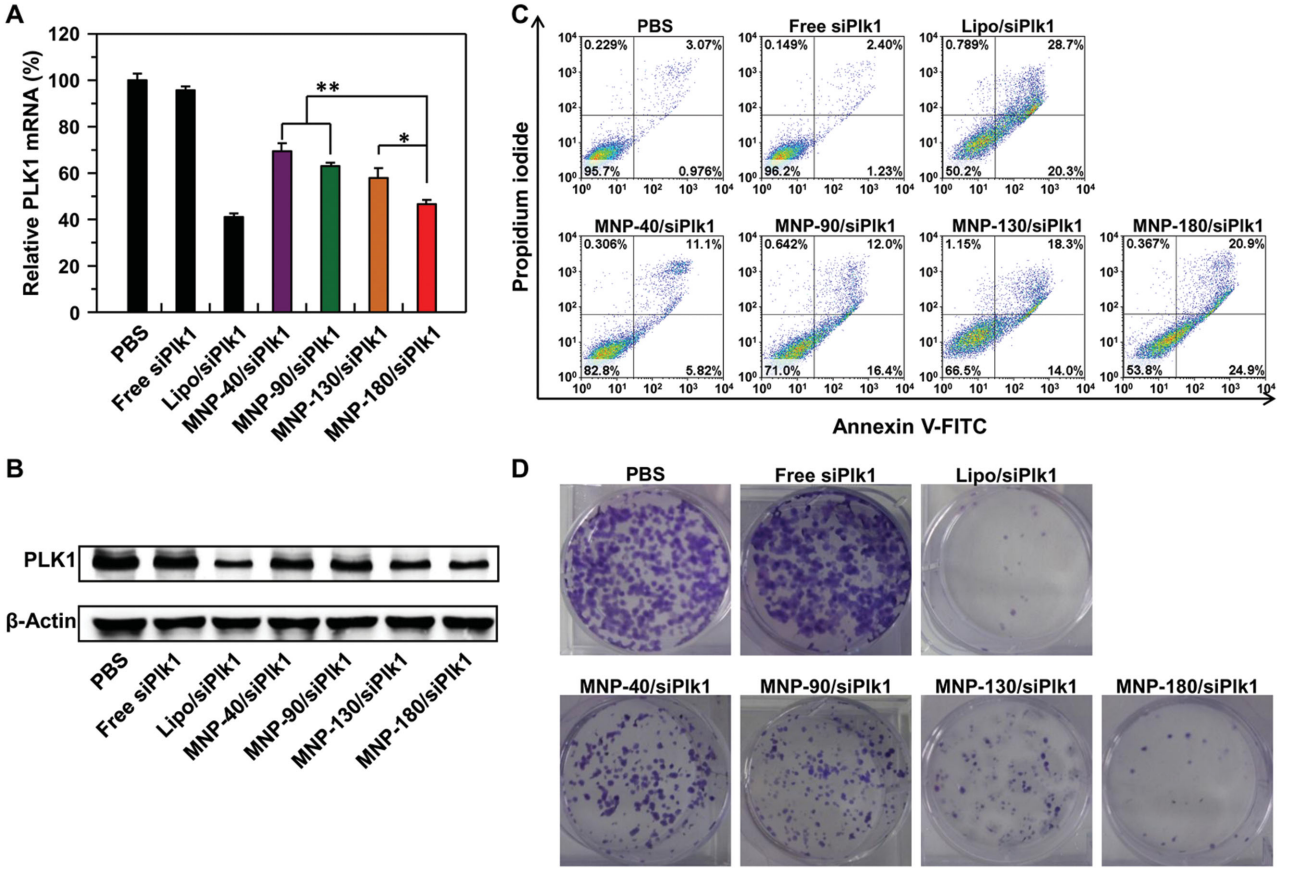

Figure 4. A,B) Expression of Plk1 mRNA A) and protein B) in MDA-MB-231 cells following incubation with different formulations. C) Induction of apoptosis in MDA-MB-231 cells following incubation with different formulations. Early apoptotic cells are shown in the lower right quadrant and late apoptotic cells are shown in the upper right quadrant. Cell apoptosis after treatment with other controls is given in the Supporting Information (Figure S7). D) Inhibition of cell proliferation in MDA-MB-231 cells after treatment with different sized MNP/siRNAs for 72 h. The number of colonies was used as a measure of cell proliferation. The final concentration of siPlk1 in the culture medium was 200×10^{-9} M in the experiments. Lipo/siPlk1 (positive control) represents complexes of LipofectamineiMAX with siPlk1 (50×10^{-9} M), and free siPlk1 (200×10^{-9} M) was used as a negative control. $^{*}p < 0.05$, $^{**}p < 0.01$ ($n = 3$).

improve the target gene silencing efficiency in MDA-MB-231 cells, which was consistent with the improved siRNA internalization seen as a result of the increased size of the MNP/siRNA (Figure 2).

The inhibition of Plk1 expression in tumor cells induced cell apoptosis and suppressed cell proliferation.[42] The enhancement of Plk1 gene silencing efficiency by increasing the size of the MNP/siRNA might result in an elevated induction of cell apoptosis and suppression of cell proliferation. To demonstrate this, after incubation with the above-mentioned formulations, apoptosis and proliferation were analyzed by annexin V-FITC/PI staining and colony formation assay, respectively. As shown in Figure 4C, the percentage of cells suffering apoptosis (including early apoptotic cells and fully apoptotic cells) after treatment with MNP-40/siPlk1, MNP-90/siPlk1, MNP-130/siPlk1, or MNP-180/siPlk1 was 16.92%, 28.40%, 32.30%, and 45.80%, respectively. On the contrary, treatment of MDA-MB-231 cells with differently sized MNP/siN.C. or free siPlk1 did not induce remark apoptosis when compared with PBS group. Similarly, no significant inhibition of cells proliferation was observed upon treatment with free siPlk1 or the different sized MNP/siN.C, while different sized MNP/siPlk1 significantly inhibited the growth of MDA-MB-231 cells in a size-dependent manner (Figure 4D). Therefore, based on the above results (from Figures 2 to 4), it can be summarized that the increased size of MNP/siRNA enhanced cellular uptake by endocytosis in MDA-MB-231 cells, thus improving the gene silencing efficiency and subsequently enhancing the inhibition of cell proliferation and elevating cell apoptosis.

2.5. 90 nm MNP/siRNAs Exhibit the Best Gene Silencing Efficiency and Highest Antitumor Efficacy

According to the results of the cell experiments, we speculated that treatment with different sized MNP/siRNA should show size-dependent antitumor efficacies in a tumor model. To demonstrate this, MDA-MB-231 tumor-bearing mice were randomly divided into different groups and treated with PBS, free siPlk1, and different sized MNP/siPlk1 or MNP/siN.C. at an siRNA dose of 10 μg per injection every other day. The most efficient tumor inhibition was detected after intravenous injection of

© 2015 WILEY-VCH Verlag GmbH & Co. KGaA, Weinheim

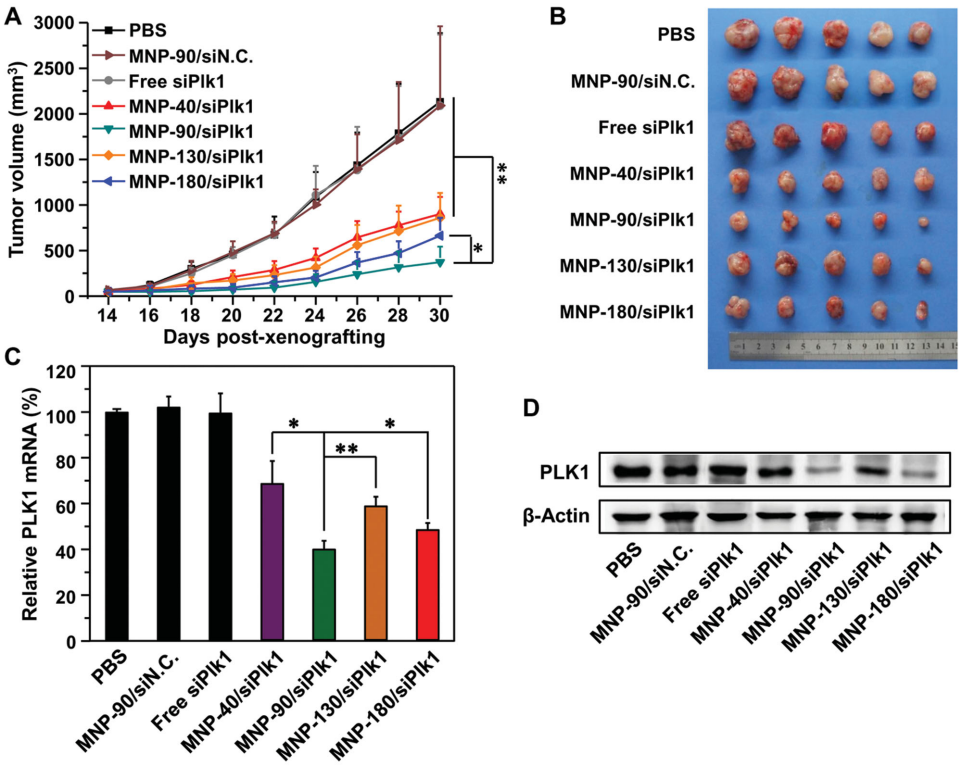

Figure 5. A) Inhibition of tumor growth in a murine model with MDA-MB-231 xenografts after treatment with various formulations ($n = 6$). B) Images of MDA-MB-231 xenograft tumors at the end of the treatment. C,D) Expression of Plk1 mRNA C) and protein D) in tumors analyzed 24 h after the final injection. MDA-MB-231 xenograft tumor-bearing mice received one intravenous injection every day from the 14th day postxenograft implantation onward in all of the experiments. The dose of siRNA was 10 μg per injection every other day. *$p < 0.05$, **$p < 0.01$ ($n = 6$).

MNP-90/siPlk1, and tumor growth was moderately inhibited by intravenous injection of MNP-40/siPlk1, MNP-130/siPlk1, and MNP-180/siPlk1 (**Figure 5**A,B). This result was a surprise because gene silencing efficiency and cell apoptosis were moderate for MNP-90/siPlk1. To further confirm this result, Plk1 expression at the mRNA and protein levels in the tumors were analyzed by RT-PCR and Western blot analyses, respectively, following the treatment. As shown in Figure 5C, after treatment with MNP-40/siPlk1, MNP-90/siPlk1, MNP-130/siPlk1, and MNP-180/siPlk1, Plk1 mRNA levels showed a 32.0 ± 10.0%, 60.6 ± 3.8%, 41.7 ± 4.2%, and 52.1 ± 3.1% reduction, respectively, when compared to the level in tumors following treatments with PBS. Moreover, the Plk1 protein displayed a consistent knockdown efficiency in each group. As shown in Figure 5D, only slight down-regulation of Plk1 protein expression was detected after administration of MNP-40/siPlk1 and MNP-130/siPlk1. However, the most significant downregulation of Plk1 protein expression occurred when the mice were treated with the MNP-90/siPlk1, which was further confirmed by immunohistochemistry analyses of Plk1 protein in the tumor tissue (Figure S8, Supporting Information). Moreover, cell proliferation and apoptosis in the tumor tissues were analyzed by immunohistochemical staining after the treatment. As shown in Figure S8 (Supporting Information), treatment with MNP-90/siPlk1 was demonstrated to be the most effective formulation in reducing the percentage of proliferating Ki67-positive tumor cells and increasing TUNEL-positive tumor cells, indicating the optimal efficiency of the MNP-90/siPlk1 treatment in inducing apoptosis and inhibiting tumor cell proliferation. The above results demonstrated that MDA-MB-231 tumors in mice treated with MNP-90/siPlk1 exhibited the best antitumor effects, due to the preparation's improved Plk1 gene silencing efficiency resulting in its greatest efficiency in induction of tumor apoptosis.

2.6. 90 nm MNPs Show the Optimal Balance of Prolonged Circulation and Cellular Uptake by Tumor Cells, Thus Exhibiting the Highest Retention in Tumors

The size effect of MNP/siRNA on antitumor efficacies showed differences when compared with the in vitro results, due to the different gene silencing efficiencies of these MNP/siRNAs in vitro and in vivo. The in vitro gene silencing efficiency indicated that increasing the size of the MNP/siRNA leads to improved target gene silencing efficiency due to the enhanced cellular uptake. However, among these MNP/siRNAs, treatment with the MNP-90/siPlk1 exhibited the best Plk1 gene silencing efficiency in tumors, which may be because siRNA carried by MNP-90 was taken up most efficiently by tumor cells in vivo after systemic delivery. As reported, the circulation and accumulation of nano-drug delivery systems following systemic administration are a prerequisite for cellular uptake by the tumor cells via endocytosis. Therefore, the circulation and accumulation of these MNP/siRNAs might be the main factors resulting in their different anticancer efficiencies in vitro

© 2015 WILEY-VCH Verlag GmbH & Co. KGaA, Weinheim

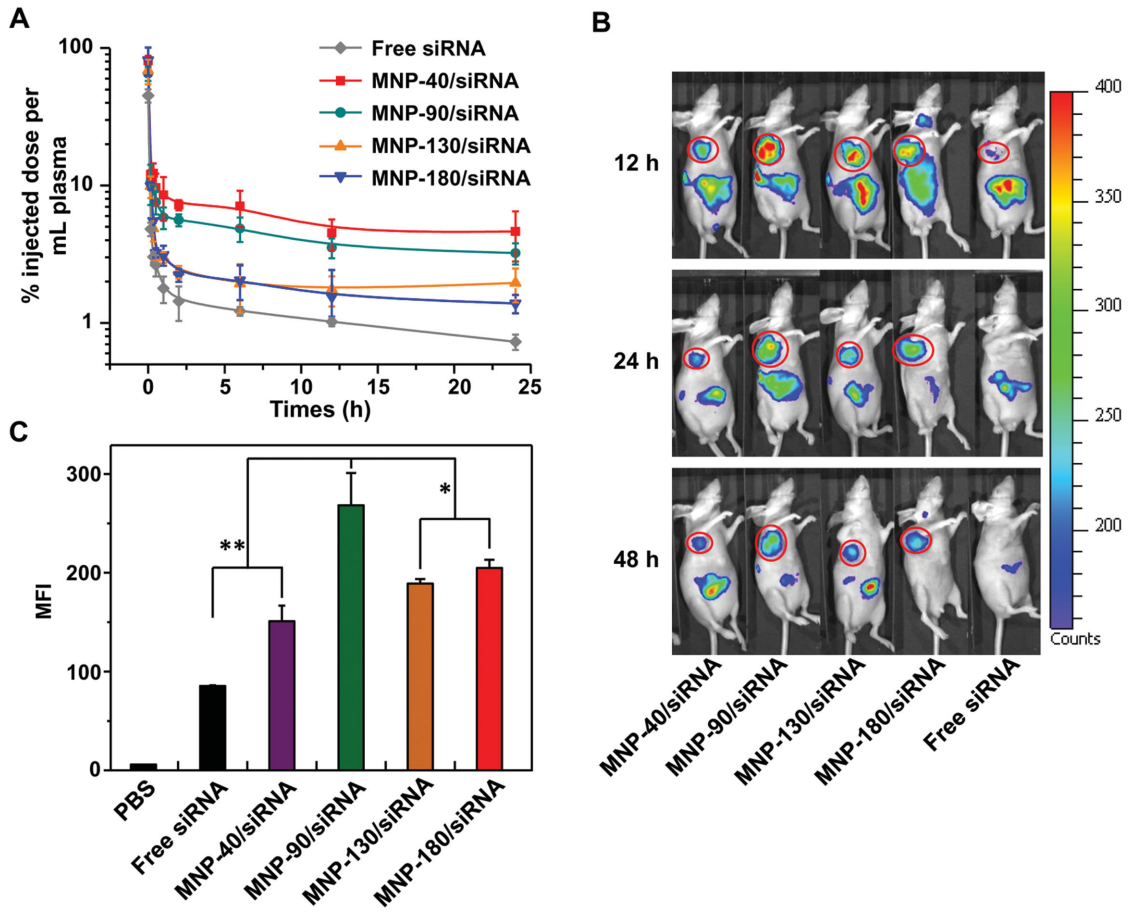

Figure 6. A) Plasma siRNA concentration versus time after intravenous injection of different sized MNP/siRNAs and free siRNA at a dose of 40 μg per mouse (mean ± SD, $n = 4$). B) Distribution of Cy5-siRNA in MDA-MB-231 xenograft-bearing mice after 12, 24, and 48 h postadministration of different formulations. The injected dose of Cy5-siRNA was 40 μg per mouse. C) Mean fluorescence intensity (MFI) of Cy5-siRNA in GFP-expressing MDA-MB-231 cells that were separated from tumor tissue. Different sized MNP/Cy5-siRNAs, or equivalent free Cy5-siRNA (40 μg per mouse), were intravenously administered and the GFP-expressing MDA-MB-231 cells were isolated for flow cytometric analyses. $^{*}p < 0.05$, $^{**}p < 0.01$ ($n = 6$).

and in vivo. To verify this speculation, the pharmacokinetics and accumulation of these MNP/siRNAs were examined. After intravenous injection of the MNP/siRNAs, blood was collected at 0 min, 10 min, 20 min, 30 min, 1 h, 2 h, 6 h, 12 h, and 24 h, and the plasma siRNA concentration was determined by HPLC according to our previously reported method.[43] As shown in **Figure 6**A, free siRNA was eliminated rapidly after intravenous injection. Among the MNP/siRNAs, the size-dependence of clearance was evident; with MNP-40/siRNA ($T_{1/2}$: 47.19 ± 15.82 h) possessing the longest half-time in blood circulation, MNP-90/siRNA ($T_{1/2}$: 28.73 ± 2.26 h) having a slightly reduced blood circulation, and the MNP-130/siRNA ($T_{1/2}$: 16.66 ± 1.70 h) and MNP-180/siRNA ($T_{1/2}$: 18.78 ± 5.82 h) being cleared away more rapidly compared with MNP-40/siRNA and MNP-90/siRNA. Meanwhile, the MNP-90/siRNA nanoparticles most significantly increased the area under the curve (AUC) in blood, which was 2.39-fold greater compared to MNP-180/siRNA. This size-dependent clearance may be due to increased uptake by macrophages (Figure S9, Supporting Information) as the size of the MNP/siRNA increased.

Furthermore, to demonstrate the size effect on accumulation in vivo, we examined the biodistribution of siRNA in the tumor following intravenous injection of the above-mentioned formulations into nude mice bearing the MDA-MB-231 tumor model. The distribution was analyzed after 12, 24, and 48 h postadministration through the fluorescence signal collected by a Xenogen IVIS Lumina system. As shown in Figure 6B, the MNP-90/siRNA showed the highest accumulation in tumors at all time points, followed by MNP-180/siRNA, MNP-130/siRNA, and MNP-40/siRNA. This result does not seem to be consistent with the circulation of these MNP/siRNAs. It seems reasonable that delivery of siRNA with MNP-40 should show the highest siRNA accumulation in tumors because it prolonged the circulation time of the siRNA most efficiently (Figure 6A). However, it should be noted that although the smaller sized MNP/siRNAs resulted in an increased amount of siRNA circulating within the tumor interstitials due to avoiding uptake by macrophages (Figure S9, Supporting Information), the smaller size of these MNP/siRNAs also meant they were less readily taken up by tumor cells, but rather were subsequently eliminated by the lymphatic system. Therefore, there must be a balance between the cellular uptake of the different sized MNP/siRNAs and their circulation, and 90 nm MNPs are the optimal size for these siRNA-loaded nanoparticles. Thus, the greatest amount of

© 2015 WILEY-VCH Verlag GmbH & Co. KGaA, Weinheim

siRNA was delivered to tumor cells following intravenous injection of MNP-90/siRNAs.

To demonstrate this, we further detected the amount of intracellular siRNA in vivo in a murine model of GFP-expressing MDA-MB-231/GFP cells; thus, the GFP protein can function as an indicator for particular tumor cells. Cy5-labeled siRNA (red) was used to highlight the different sized MNPs, and the GFP-expressing MDA-MB-231 cells (green) were isolated in order to analyze the Cy5-siRNA florescence in the GFP-expressing cells by flow cytometry. As shown in Figure 6C, the strongest fluorescence intensity in MDA-MB-231/GFP cells was observed 48 h after intravenous injection of MNP-90/Cy5-siRNA, and the intracellular fluorescence intensity was reduced in turn after treatment with MNP-180/Cy5-siRNA, MNP-130/Cy5-siRNA, and MNP-40/Cy5-siRNA. The highest cellular uptake of Cy5-siRNA by tumor cells being achieved following intravenous injection of MNP-90/Cy5-siRNA was further corroborated by CLSM (Figure S10, Supporting Information). The strongest red fluorescent signal from the siRNA was detected in tumor tissue sections exposed to MNP-90/Cy5-siRNA when compared to administration of other sized MNP/Cy5-siRNA. These results verified that 90 nm MNPs are the optimal size for delivery of siRNA, as they most efficiently facilitated cellular uptake by tumor cells following accumulation in MDA-MB-231 tumor tissue, and further enhanced the antitumor efficacy.

3. Conclusion

To investigate the optimal size of nanocarriers for siRNA delivery, we have rationally designed different sized MNP/siRNAs. We systematically evaluated the size effect on circulation, internalization, retention, and overall antitumor efficacy. The results from in vitro and in vivo experiments clearly demonstrated that the size of nanocarriers used for siRNA delivery plays a critical role in determining their biological properties and antitumor activity. The 90 nm MNPs showed the most significant antitumor efficacy in a MDA-MB-231 xenograft murine model due to possessing the highest siRNA retention and best gene silencing efficacy following intravenous injection. In contrast, the larger MNPs (130 and 180 nm) were rapidly cleared from the circulation and the smaller MNPs (40 nm) were inefficiently taken up by tumor cells, leading to overall low gene silencing efficacy and antitumor efficacy. Therefore, 90 nm was the optimal balance of prolonged circulation and cellular uptake by tumor cells among these different sized nanocarriers, indicating that 90 nm could be at or close to the optimal size for systemic delivery of siRNA in a MDA-MB-231 xenograft murine model. Our findings provide valuable information and methodology for the rational design of the next generation of siRNA delivery systems, which achieve better therapeutic effects in cancer therapy.

4. Experimental Section

Materials: Dulbecco's modified Eagle's medium (DMEM) and trypsin-EDTA were purchased from Gibco BRL (Eggenstein, Germany). FBS, the Lipofectamine RNAiMAX transfection kit, DAPI, and Alexa Fluor 488 phalloidin were provided by Invitrogen (Carlsbad, NM). *N*-2-hydroxyethylpiperazine-*N'*-2-ethanesulfonic acid buffered saline (HEPES), collagenase I, RNase A, and heparin sulfate were purchased from Sigma-Aldrich Co. (Shanghai, China). The CellTiter 96 Aqueous One Solution Cell Proliferation Assay used for the methyl thiazol tetrazolium (MTT) assay was purchased from Promega Biotech. Co. Ltd. (Beijing, China). The fluorescent-labeled FAM-siRNA, Cy5-siRNA, negative control siRNA with a scrambled sequence (siN.C., antisense strand, 5′-AACCACTCAACTTTTTCCCAAdTdT-3′), and siRNA-targeting Plk1 mRNA (siPlk1, antisense strand, 5′-UAAGGAGGGUGAUCUUCUUCAdTdT-3′) were supplied by Suzhou Ribo Life Science Co. (Kunshan, China). Other organic solvents or reagents were analytical grade and used as received.

Preparation of Different Sized MNPs: Different sized cationic MNPs were prepared by changing the molar ratios of mPEG-*b*-PCL, PCL-*b*-PPEEA, and homopolymer PCL using a dialysis method. In the present work, we synthesized the polymer $mPEG_{114}$-*b*-PCL_{41}, PCL_{25}-*b*-$PPEEA_{17}$, or PCL_{34} (the subscript number represents degree of polymerization of each block) using a previously reported procedure, and the characterization was provided in the Supporting Information.[36] $mPEG_{114}$-*b*-PCL_{41} (10 mg), PCL_{25}-*b*-$PPEEA_{17}$ (10 mg), or PCL_{34} (50 mg) were dissolved in 1 mL of solution (acetonitrile:methyl alcohol = 1:1). The molar ratio of $mPEG_{114}$-*b*-PCL_{41} and PCL_{25}-*b*-$PPEEA_{17}$ was maintained at 1.5:1, and PCL_{34} was gradually added into the mixed solution in different molar ratios. Then, the mixed solution was stirred gently at room temperature for 15 min and added to ultrapurified water (Millipore, 18.2 MΩ) that was ten times the volume of the organic solvent. After stirring again at room temperature for 20 min, the solution was transferred into a rotary evaporator (Buchi, Switzerland) and rotated for 15–20 min to completely remove the organic solvent. The diameters and zeta potentials of the MNPs were analyzed by a Malvern Zetasizer Nano ZS90 apparatus at 25 °C, illuminating the sample with 633 nm wavelength radiation from a solid-state He–Ne laser and collecting the scattered light at an angle of 90°. The MNPs were analyzed in triplicate at a concentration of 1.0 mg mL^{-1}. The morphology of the MNPs was examined by JEOL-2010 TEM (Tokyo, Japan) at an accelerating voltage of 200 kV.

Preparation of Different Sized MNP/siRNA Complexes and Gel Retardation Assay: For siRNA binding, the different sized MNPs were diluted to different concentrations for the desired N:P ratios, added to the siRNA solution (20×10^{-3} M), and incubated a further 20 min to allow formation of the MNP/siRNA complexes. The formed complexes were electrophoresed on a 1% agarose gel at 120 mV for 10 min in Tris/borate/EDTA buffer (TBE buffer; 89×10^{-3} M Tris, 89×10^{-3} M boric acid, 2×10^{-3} M EDTA, pH 8.3). The siRNA bands were visualized with ethidium bromide staining under a UV transilluminator (Tanon GIS System, Shanghai, China) at a wavelength of 365 nm. Free siRNA was used as the control. The mean diameters and surface zeta potentials of the MNP/siRNA complexes at different N:P ratios were monitored as described above.

In Vitro siRNA Release: Different sized MNP/FAM-siRNAs prepared at an N/P ratio of 10:1 were suspended in PBS (0.02 M, pH 7.4 or 5.5) at a siRNA concentration of 200 pmol mL^{-1} and incubated at 37 °C with gentle shaking. At different time intervals, samples were taken and centrifuged (30 000 ×*g*, 1 h). The concentration of FAM-siRNA in the supernatant was determined by HPLC and the amount of FAM-siRNA released was calculated accordingly.[35]

Determining the Stability of Different Sized MNP/siRNAs: MNP/siRNAs prepared at an N/P ratio of 10:1 were incubated in DMEM with 10% FBS (pH 7.4) at 37 °C under gentle stirring. At each time point, the mean diameters of the micelleplex were monitored by a Malvern Zetasizer Nano ZS90 apparatus as described above.

Cell Culture: The human breast cancer MDA-MB-231 cells were obtained from the American Type Culture Collection (ATCC) and maintained in DMEM supplemented with 10% FBS. Cells were incubated at 37 °C in a 5% CO_2 atmosphere.

Cellular Uptake of Different Sized MNP/siRNAs: For microscopic observation, MDA-MB-231 cells were seeded into 24-well plates at 5×10^4 cells per well in 0.5 mL of complete DMEM and cultured at 37 °C in a 5% CO_2 humidified atmosphere for 24 h. Then, free FAM-siRNA

© 2015 WILEY-VCH Verlag GmbH & Co. KGaA, Weinheim

or different sized MNP/FAM-siRNAs were added and the final FAM-siRNA concentration in the culture medium adjusted to 200×10^{-9} M. After further incubation for 4 h, the cells were washed twice with PBS and fixed with 4% paraformaldehyde for 15 min at room temperature for flow cytometry analyses (FACS Calibur flow cytometer, BD Biosciences, USA). The cells were stained with Alexa Fluor 568 phalloidin (Invitrogen, Carlsbad, CA) and DAPI to counterstain the cytoskeleton and cell nuclei according to the standard protocol provided by the suppliers. To reduce fluorescent photobleaching, the coverslips were mounted on glass microscope slides with a drop of anti-fade mounting medium (Sigma-Aldrich). The cellular uptake was observed by CLSM (LSM 710, Carl Zeiss, Inc., Jena, Germany). For flow cytometric analysis, MDA-MB-231 cells were seeded into 24-well plates at 1×10^5 cells per well in 0.5 mL of complete DMEM medium and cultured at 37 °C in a 5% CO_2 humidified atmosphere for 24 h. Then, the cells were incubated with the above formulations. After further incubation for 4 h, the cells were washed twice with cold PBS (pH 7.4), trypsinized, washed with cold PBS (pH 7.4), filtered through 35 μm nylon mesh, and subjected to flow cytometric analysis using a BD FACSCalibur flow cytometer (BD Bioscience, Bedford, MA). The results were analyzed using Flowjo 7.6.1 software. For HPLC analyses, MDA-MB-231 cells were incubated with the above formulations for 4 h. Subsequently, the cells were washed twice with PBS, and lysed with 1% Triton X-100 in PBS (250 μL) at 37 °C for 30 min, followed by three freeze–thaw cycles. Then, polyanionic heparin (MW = 17–19 k, Sigma, 1 mg mL^{-1}) was added to induce decomplexation and the lysates were further incubated 30 min. The concentration of FAM-siRNA in the cell lysates was measured by HPLC according to a previously reported method.[43]

Cellular Uptake Mechanism: MDA-MB-231 cells were seeded into 24-well plates at 1×10^5 cells per well in 0.5 mL of complete DMEM medium and cultured at 37 °C in a 5% CO_2 humidified atmosphere for 24 h. Then, the cells were incubated at either 37 °C or at 4 °C. Prior to incubation with different sized MNP/siRNAs at 37 °C, the cells were pretreated with wortmannin (10×10^{-6} M, Sigma-Aldrich Co., USA), sucrose (0.45 M, Invitrogen, USA), or filipin (5 μg mL^{-1}, Sigma-Aldrich Co., USA) as previously reported. After incubation with the above formulations for 4 h, the cells were analyzed by flow cytometry as described above.

In Vitro Transfection and Analysis of Gene Expression: MDA-MB-231 cells (2×10^5) were seeded in a six-well tissue culture plate and cultured at 37 °C in a 5% CO_2 humidified atmosphere for 24 h. Then, the cells were treated with different sized MNP/siRNAs encapsulating siPlk1 or siN.C. at a dose of 200×10^{-9} M. Free siPlk1 was used as a negative control, and Lipofectamine RNAiMAX carrying siPlk1 (Lipo/siPlk1) at a dose of 50×10^{-9} M was used as the positive control. After incubation for 48 h (for mRNA isolation) or 72 h (for protein extraction) at 37 °C, the cellular levels of Plk1 mRNA and protein were assessed using quantitative reverse transcription real-time PCR (qRT-PCR) and Western blotting, respectively, and a procedure that has been reported previously.[44]

Cell Apoptosis and Proliferation Analysis: For the cell apoptosis analysis, MDA-MB-231 cells were seeded into six-well plates (2×10^5 per well) and incubated for 24 h. The cells were then treated with the above formulations for 96 h. Then, the cells were collected and the apoptotic cells were detected by flow cytometry using the annexin V-FITC apoptosis detection kit I (BD Biosciences, San Diego, CA) according to the standard protocol provided by the suppliers. The results were analyzed using Flowjo 7.6.1 software. A colony formation assay was used to detect cell proliferation. MDA-MB-231 cells were treated with the above formulations for 48 h, then trypsinized and resuspended in DMEM medium. One thousand cells were plated in each well of a six-well plate. The cells were further incubated at 37 °C with 5% CO_2 for 10 d to observe the colony formation.

Xenograft Tumor Model: BALB/nu-nu nude mice (6 weeks old) were purchased from Vital River Laboratories (Beijing, China) and all animals received care in compliance with the guidelines outlined in the Guide for the Care and Use of Laboratory Animals. The procedures were approved by the University of Science and Technology of China's Animal Care and Use Committee. The xenograft tumor model was generated by injecting MDA-MB-231 cells (2×10^6 per mouse) in the mammary fat pad of each mouse. The green fluorescent protein-expressing xenograft tumor model was generated by subcutaneous injection of MDA-MB-231 cells stably expressing GFP (2×10^6 per mouse) in the mammary fat pad of each mouse as previously described.[45]

Pharmacokinetics Studies: Different sized MNP/siRNAs carrying FAM-siRNA were intravenously injected into ICR mice (Vital River Laboratories, Beijing, China) at a siRNA dose of 40 μg per mouse ($n = 4$ for each group). Blood samples were collected at the predetermined time points, and the concentration of FAM-siRNA in the plasma was analyzed by HPLC using a previously reported method.[43] The pharmacokinetics parameters were calculated by DAS 3.0 with the noncompartmental model.

Accumulation of siRNA in Tumor Tissue and In Vivo Cellular Uptake: When the MDA-MB-231 tumor volume was about 200 mm^3, the mice were intravenously injected with 200 μL of different sized MNP/siRNAs carrying 40 μg Cy5-siRNA or free Cy5-siRNA. The mice were anesthetized at the predetermined time points and imaged by a Xenogen IVIS Lumina system (Caliper Life Sciences, USA). The results were analyzed using Living Image 3.1 software (Caliper Life Sciences). To further examine the in vivo cellular uptake of different sized MNP/siRNAs by tumor cells, a stable GFP-expressing xenograft tumor model was used. Tumor tissue cells were separated at 48 h postinjection of the above formulations as described above. The fluorescence of the GFP-labeled tumor cells was analyzed by flow cytometry. The amplification scale was logarithmic for the FL1-H and FL4-H parameters and linear for SSC-H and FSC-H. MDA-MB-231 tumor cells stably expressing GFP were carefully gated out using FL1-H versus SSC-H bivariant graphs. Within this gate, the geometric MFI of GFP positive cells was determined in the FL4-H histogram. For microscopic observation of Cy5-siRNA distribution in tumor tissue, tumor tissues were collected at 48 h postinjection, frozen, and sectioned. Sections were counterstained with DAPI for the cell nucleus and Alexa Fluor 488 phalloidin for the cytoskeleton following the manufacturer's instructions. The slides were analyzed using LCSM.

Tumor Suppression Study: When the tumor volume was around 100 mm^3 14 d after MDA-MB-231 cell implantation, the mice were randomly divided into six groups and treated once every other day with PBS, different sized MNP/siPlk1 or, in the case of the control group, with an equivalent siRNA dose of 10 μg per injection per mouse. The volume of the tumor was monitored every other day and calculated according to the formula: tumor volume (mm^3) = $0.5 \times \text{length} \times \text{width}^2$.

Detection of Plk1 Expression in Tumor Tissue: Tumor tissues were excised 48 h after the last intravenous injection. For Plk1 mRNA analysis, a piece of tumor tissue (≈10 mg) was triturated and detected by qRT-PCR. For Plk1 protein analysis, a piece of tumor tissue (≈50 mg) was triturated and detected by Western blot analysis using a previously reported method.[44]

Statistical Analysis: The statistical significance of treatment outcomes was assessed using the Student's t-test; $p < 0.05$ was considered statistically significant in all analyses (95% confidence level).

Supporting Information

Supporting Information is available from the Wiley Online Library or from the author.

Acknowledgements

This work was supported by the National Basic Research Program of China (973 Programs, 2013CB933900, 2015CB932100, and 2012CB932500), the National High Technology Research and Development Program of China (863 Programs, 2012AA022501), and the National Natural Science Foundation of China (51125012, 51390482, 51203145, 81272897).

Received: April 17, 2015
Revised: May 25, 2015
Published online: June 25, 2015

© 2015 WILEY-VCH Verlag GmbH & Co. KGaA, Weinheim

[1] A. Fire, S. Q. Xu, M. K. Montgomery, S. A. Kostas, S. E. Driver, C. C. Mello, *Nature* **1998**, *391*, 806.
[2] M. E. Davis, J. E. Zuckerman, C. H. J. Choi, D. Seligson, A. Tolcher, C. A. Alabi, Y. Yen, J. D. Heidel, A. Ribas, *Nature* **2010**, *464*, 1067.
[3] C. V. Pecot, G. A. Calin, R. L. Coleman, G. Lopez-Berestein, A. K. Sood, *Nat. Rev. Cancer* **2011**, *11*, 59.
[4] D. Bumcrot, M. Manoharan, V. Koteliansky, D. W. Y. Sah, *Nat. Chem. Biol.* **2006**, *2*, 711.
[5] X. Guo, L. Huang, *Acc. Chem. Res.* **2012**, *45*, 971.
[6] R. Kanasty, J. R. Dorkin, A. Vegas, D. Anderson, *Nat. Mater.* **2013**, *12*, 967.
[7] F. H. Meng, W. E. Hennink, Z. Zhong, *Biomaterials* **2009**, *30*, 2180.
[8] L. Han, J. Zhao, X. Zhang, W. Cao, X. Hu, G. Zou, X. Duan, X. J. Liang, *ACS Nano* **2012**, *6*, 7340.
[9] N. P. Gabrielson, H. Lu, L. Yin, K. H. Kim, J. Cheng, *Mol. Ther.* **2012**, *20*, 1599.
[10] A. S. Malamas, M. Gujrati, C. M. Kummitha, R. Xu, Z. R. Lu, *J. Controlled Release* **2013**, *171*, 296.
[11] C. Zheng, M. Zheng, P. Gong, J. Deng, H. Yi, P. Zhang, Y. Zhang, P. Liu, Y. Ma, L. Cai, *Biomaterials* **2013**, *34*, 3431.
[12] Z. X. Zhao, S. Y. Gao, J. C. Wang, C. J. Chen, E. Y. Zhao, W. J. Hou, Q. Feng, L. Y. Gao, X. Y. Liu, L. R. Zhang, Q. Zhang, *Biomaterials* **2012**, *33*, 6793.
[13] Y. Li, R. Liu, J. Yang, G. Ma, Z. Zhang, X. Zhang, *Biomaterials* **2014**, *35*, 9731.
[14] J. G. Li, X. S. Yu, Y. Wang, Y. Y. Yuan, H. Xiao, D. Cheng, X. T. Shuai, *Adv. Mater.* **2014**, *26*, 8217.
[15] M. E. Davis, Z. Chen, D. M. Shin, *Nat. Rev. Drug Discovery* **2008**, *7*, 771.
[16] H. Hatakeyama, H. Akita, H. Harashima, *Adv. Drug Delivery Rev.* **2011**, *63*, 152.
[17] K. M. Choi, S. H. Choi, H. Jeon, I. S. Kim, H. J. Ahn, *ACS Nano* **2011**, *5*, 8690.
[18] M. L. Patil, M. Zhang, T. Minko, *ACS Nano* **2011**, *5*, 1877.
[19] A. Akinc, A. Zumbuehl, M. Goldberg, E. S. Leshchiner, V. Busini, N. Hossain, S. A. Bacallado, D. N. Nguyen, J. Fuller, R. Alvarez, A. Borodovsky, T. Borland, R. Constien, A. de Fougerolles, J. R. Dorkin, K. N. Jayaprakash, M. Jayaraman, M. John, V. Koteliansky, M. Manoharan, L. Nechev, J. Qin, T. Racie, D. Raitcheva, K. G. Rajeev, D. W. Y. Sah, J. Soutschek, I. Toudjarska, H. P. Vornlocher, T. S. Zimmermann, R. Langer, D. G. Anderson, *Nat. Biotechnol.* **2008**, *26*, 561.
[20] M. Khan, C. Y. Ang, N. Wiradharma, L. K. Yong, S. Liu, L. Liu, S. Gao, Y. Y. Yang, *Biomaterials* **2012**, *33*, 4673.
[21] D. C. Forbes, N. A. Peppas, *ACS Nano* **2014**, *8*, 2908.
[22] Y. Geng, P. Dalhaimer, S. S. Cai, R. Tsai, M. Tewari, T. Minko, D. E. Discher, *Nat. Nanotechnol.* **2007**, *2*, 249.
[23] E. C. Cho, J. Xie, P. A. Wurm, Y. Xia, *Nano Lett.* **2009**, *9*, 1080.
[24] D. L. J. Thorek, A. Tsourkas, *Biomaterials* **2008**, *29*, 3583.
[25] A. Albanese, P. S. Tang, W. C. W. Chan, *Annu. Rev. Biomed. Eng.* **2012**, *14*, 1.
[26] S. E. A. Gratton, P. A. Ropp, P. D. Pohlhaus, J. C. Luft, V. J. Madden, M. E. Napier, J. M. DeSimone, *Proc. Natl. Acad. Sci. U.S.A.* **2008**, *105*, 11613.
[27] W. Jiang, B. Y. S. Kim, J. T. Rutka, W. C. W. Chan, *Nat. Nanotechnol.* **2008**, *3*, 145.
[28] H. Jin, D. A. Heller, R. Sharma, M. S. Strano, *ACS Nano* **2009**, *3*, 149.
[29] C. D. Walkey, J. B. Olsen, H. Guo, A. Emili, W. C. W. Chan, *J. Am. Chem. Soc.* **2012**, *134*, 2139.
[30] P. Zhao, M. Zheng, C. Yue, Z. Luo, P. Gong, G. Gao, Z. Sheng, C. Zheng, L. Cai, *Biomaterials* **2014**, *35*, 6037.
[31] H. Cabral, Y. Matsumoto, K. Mizuno, Q. Chen, M. Murakami, M. Kimura, Y. Terada, M. R. Kano, K. Miyazono, M. Uesaka, N. Nishiyama, K. Kataoka, *Nat. Nanotechnol.* **2011**, *6*, 815.
[32] L. Tang, X. Yang, Q. Yin, K. Cai, H. Wang, I. Chaudhury, C. Yao, Q. Zhou, M. Kwon, J. A. Hartman, I. T. Dobrucki, L. W. Dobrucki, L. B. Borst, S. Lezmig, W. G. Helferich, A. L. Ferguson, T. M. Fan, J. Cheng, *Proc. Natl. Acad. Sci. U.S.A.* **2014**, *111*, 15344.
[33] C. Q. Mao, M. H. Xiong, Y. Liu, S. Shen, X. J. Du, X. Z. Yang, S. Dou, P. Z. Zhang, J. Wang, *Mol. Ther.* **2014**, *22*, 964.
[34] Y. C. Ma, J. X. Wang, W. Tao, H. S. Qian, X. Z. Yang, *ACS Appl. Mater. Interfaces* **2014**, *6*, 16174.
[35] X. Z. Yang, S. Dou, T. M. Sun, C. Q. Mao, H. X. Wang, J. Wang, *J. Controlled Release* **2011**, *156*, 203.
[36] H. X. Wang, M. H. Xiong, Y. C. Wang, J. Zhu, J. Wang, *J. Controlled Release* **2013**, *166*, 106.
[37] N. W. S. Kam, Z. A. Liu, H. J. Dai, *Angew. Chem. Int. Ed.* **2006**, *45*, 577.
[38] J. Rejman, A. Bragonzi, M. Conese, *Mol. Ther.* **2005**, *12*, 468.
[39] T. Luehmann, M. Rimann, A. G. Bitterman, H. Hall, *Bioconjugate Chem.* **2008**, *19*, 1907.
[40] A. D. Judge, M. Robbins, I. Tavakoli, J. Levi, L. Hu, A. Fronda, E. Ambegia, K. McClintock, I. MacLachlan, *J. Clin. Invest.* **2009**, *119*, 661.
[41] Y. Bu, Z. Yang, Q. Li, F. Song, *Oncology* **2008**, *74*, 198.
[42] X. Q. Liu, R. L. Erikson, *Proc. Natl. Acad. Sci. U.S.A.* **2003**, *100*, 5789.
[43] H. X. Wang, X. Z. Yang, C. Y. Sun, C. Q. Mao, Y. H. Zhu, J. Wang, *Biomaterials* **2014**, *35*, 7622.
[44] X. Z. Yang, J. Z. Du, S. Dou, C. Q. Mao, H. Y. Long, J. Wang, *ACS Nano* **2012**, *6*, 771.
[45] C. Y. Sun, S. Dou, J. Z. Du, X. Z. Yang, Y. P. Li, J. Wang, *Adv. Healthcare Mater.* **2014**, *3*, 261.

© 2015 WILEY-VCH Verlag GmbH & Co. KGaA, Weinheim